

# Nonextensivity: from low-dimensional maps to Hamiltonian systems

Constantino Tsallis<sup>1</sup>, Andrea Rapisarda<sup>2</sup>, Vito Latora<sup>2</sup>, and Fulvio Baldovin<sup>1</sup>

<sup>1</sup> Centro Brasileiro de Pesquisas Físicas,

Rua Xavier Sigaud 150, 22290-180 Rio de Janeiro, RJ, Brazil

<sup>2</sup> Dipartimento di Fisica e Astronomia and Infn Università di Catania,

Corso Italia 57, 95129 Catania, Italy

**Abstract.** We present a brief pedagogical guided tour of the most recent applications of nextensive statistical mechanics to well defined nonlinear dynamical systems, ranging from one-dimensional dissipative maps to many-body Hamiltonian systems.

## 1 Introduction

Thermodynamics and Boltzmann-Gibbs (BG) statistical mechanics constitute central formalisms of contemporary Physics. It is therefore of extreme importance to clearly establish under what exact conditions they are expected to apply, especially in what concerns the important and ubiquitous stationary state referred to as *thermal equilibrium*. This wisdom is more subtle than it looks at first sight. For instance, surprisingly enough, it is not yet exactly known the necessary and sufficient conditions for the celebrated BG distribution to correctly describe the thermostistical state of a system (see, for instance, [1]). In order to settle such conditions, it is necessary to turn onto the microscopic dynamics of the system [2], would that be classical, quantum, relativistic, or any other one that appropriately describes the system under study.

Some of the central ingredients of BG statistical mechanics are the well known logarithmic entropy ( $S_{BG} = -k \sum_{i=1}^W p_i \ln p_i$  in general, and  $S_{BG}(\{p_i = 1/W\}) = k \ln W$  for equiprobability, where for simplicity we are referring here to the case of discrete distributions of probabilities), and its exponential weight  $p_i \propto e^{-\beta E_i}$  ( $\beta \equiv 1/kT$ ,  $\{E_i\}$  being the energy spectrum) at equilibrium. This entropy has the remarkable property of extensivity for systems which are independent. More precisely, if we have a system composed by subsystems  $A$  and  $B$  such that  $p_{ij}^{A+B} = p_i^A p_j^B$  ( $\forall(i, j)$ ), then  $S_{BG}(A+B) = S_{BG}(A) + S_{BG}(B)$ . This property is at the basis of the standard understanding of thermodynamics. Such a property is not necessarily universal because it cannot be justified on general arguments (see, for instance, [3]). Strong evidence exists nowadays that it should not be generically assumed, contrarily to a widely spread, textbook belief among not few physicists. Very specifically, the *Boltzmann principle*  $S_{BG}(\{p_i = 1/W\}) = k \ln W$  should not be used for any given specific system unless properly justified. It was Einstein [2] the first who warned about this. However, many physicists (see, for instance, [4]) have not yet done their way

through this important concept. To be more precise, let us focus on  $N$ -body classical Hamiltonian  $d$ -dimensional systems including two-body interactions which do not present any mathematical complexity (such as an infinitely attractive potential) at short distances. It is acquired by now that the usual BG thermal equilibrium correctly describes the  $t \rightarrow \infty$  stationary state for all systems whose interactions are *short-ranged* (e.g., if a two-body attractive potential decreases like  $1/r^\alpha$  with  $\alpha/d > 1$ ). In particular, in this case, it is irrelevant to consider first the  $t \rightarrow \infty$  limit and then the  $N \rightarrow \infty$  limit, or the other way around. The situation is much more subtle if we have *long-ranged* interactions (e.g.,  $0 \leq \alpha/d \leq 1$ ). In this case, the  $\lim_{N \rightarrow \infty} \lim_{t \rightarrow \infty}$  still leads to the BG equilibrium, whereas the  $\lim_{t \rightarrow \infty} \lim_{N \rightarrow \infty}$  generically does *not*. It happens, typically, that more than one basin of attraction exists in the space of the initial conditions. For some initial conditions the system directly goes to the BG stationary state; for others it first goes to a non-BG state, remains there for a time which diverges with  $N$ , and only eventually goes to the BG state. In other words, depending on the size of the system and on its specific physical time scale, it might happen that the system remains in a quasi-stationary state different from the BG one for times longer than the age of the universe. In such cases, the only physically interesting situation is the non-BG one, which, perhaps for a vast class of systems, might be the one emerging within the nonextensive statistical mechanics we shall describe in the next Section. The present paper is a tutorial review of these concepts as they naturally emerge for three simple but important classes of systems, namely, (i) one-dimensional dissipative maps (e.g., the logistic map[5,6]), (ii) two-dimensional conservative maps (e.g., the standard map[7]), and (iii) classical many-body long-range-interacting Hamiltonians (e.g., the HMF model [8,9,10,11,12] and one of its generalizations, the so called  $\alpha - XY$  model [13,14]). We shall not address here the many applications of nonextensive statistical mechanics available in the literature. The interested reader may refer to [15] for various reviews. Just as an illustration, let us mention some of those applications: turbulence [16,17], electron-positron annihilation [18], diffusion of *Hydra viridissima* [19], diffusion of quarks in gluon plasma [20], Levy and correlated anomalous diffusions [21], linguistics [22], economics [23,24], fluxes of cosmic rays [25], solar neutrinos [26], high energy particle collisions [27], self-organized criticality [28], among others. In one way or another, these phenomena seem to share long-range correlations in space/time, either long-range microscopic interactions, or long-range microscopic memory (nonmarkovian processes), or (multi)fractal boundary conditions, or, generically speaking, some mechanism which creates a scale-invariant hierarchical structure of some sort. Such possibility appears to emerge in classical many-body Hamiltonians and other nonlinear dynamical systems, everytime the Lyapunov spectrum approaches zero, hence chaos becomes impossible in the sense that the sensitivity to the initial conditions diverges less than exponentially in time, though a weak mixing can remain.

## 2 Mathematical formalism

The first and main step in order to go from BG to nonextensive thermostatics is to propose the use of an entropic form which generalizes that of BG, as follows [29]:

$$S_q \equiv k \frac{1 - \sum_{i=1}^W p_i^q}{q - 1} \quad \left( \sum_{i=1}^W p_i = 1; q \in \mathbb{R} \right). \quad (1)$$

(for simplicity, and without loss of generality, we shall adopt  $k = 1$  from now on). This nonnegative form can be conveniently rewritten as

$$S_q = \langle \ln_q \frac{1}{p_i} \rangle, \quad (2)$$

where  $\langle \dots \rangle \equiv \sum_{i=1}^W (\dots) p_i$ , and the  $q$ -*logarithm* function is defined as

$$\ln_q \equiv \frac{x^{1-q} - 1}{1 - q} \quad (\ln_1 x = \ln x; x \geq 0). \quad (3)$$

The inverse function is the  $q$ -*exponential* one, given by

$$e_q^x \equiv [1 + (1 - q)x]^{1/(1-q)} \quad (e_1^x = e^x), \quad (4)$$

solution of  $dy/dx = y^q$  with  $y(0) = 1$ .  $S_q$  satisfies several remarkable properties, such as *concavity* for all  $\{p_i\}$  ( $\forall q > 0$ ), *stability* with regard to  $\{p_i\}$  ( $\forall q > 0$ ) [30], and, for  $A$  and  $B$  independent subsystems, the following *pseudo-extensivity*:

$$S_q(A + B) = S_q(A) + S_q(B) + (1 - q)S_q(A)S_q(B), \quad (5)$$

from which the denomination *nonextensive* comes. For completeness, it is convenient to mention at this point that similar entropies are the Renyi one, defined as  $S_q^R = [\ln \sum_{i=1}^W p_i^q] / [1 - q]$ , and the normalized one  $S_q^N = S_q / [\sum_{i=1}^W p_i^q]$  (introduced independently by Abe and Rajagopal [31] and by Landsberg and Vedral [32]). Renyi entropy is very useful in the context of multifractal analysis (of non-linear chaotic systems, for example). However,  $S_q^R$  and  $S_q^N$  are *not* concave for all positive values of  $q$ , *nor* are they stable [30]. These facts constitute severe drawbacks for basing a thermodynamical formalism on them. It is however convenient to have in mind that, since they are related to each other through monotonic functions  $S_q^R = \ln[1 + (1 - q)S_q] / [1 - q]$  and  $S_q^N = S_q / [1 + (1 - q)S_q]$ , they become extremized by the *same* probability distributions (assuming the supplementary constraints for optimization to be the same).

## 3 Applications to low-dimensional maps

Low-dimensional systems are a field in which the nonextensive statistical mechanics has found one of its first and most proficuous applications. What makes

low-dimensional systems extremely attractive is the simplicity of their dynamics and the possibility to have direct access to the phase space, sometimes even to plot a visual image of the entire phase space. In fact, the iterative rules of low-dimensional maps can be easily implemented on a computer and have provided useful methods to perform “numerical experiments” to check for the validity of the nonextensive formalism. As mentioned in the previous section, the BG statistics is expected to fail when the sensitivity to initial conditions is not exponential. Therefore, different authors have looked and found applications of the nonextensive formalism to cases in which the maps have a nonstandard sensitivity to initial conditions, as indicated by the vanishing of the Lyapunov exponents. Different techniques have been produced in order to calculate the ‘entropic parameter’  $q$ , and it turns out that this parameter characterizes ‘classes of universality’ of systems, at least for some of their statistical behaviors. For pedagogical reasons here we will discuss only some of the results obtained for the logistic map, as representative of a dissipative system, and for the standard map, as an example of a conservative one.

### 3.1 Dissipative Maps: the logistic map

The logistic map is one of the simplest one-dimensional dissipative system one can imagine. It has been intensively studied and it has led to important developments in chaos theory [5]. Since it has all fundamental characteristics of non-conservative systems, the logistic map is often taken as a paradigmatic example; in other words it can be considered as the Ising model of non-linear dynamical systems. The logistic map can be described by the following iterative rule<sup>1</sup>

$$x_{t+1} = f_a(x_t) = 1 - ax_t^2 \quad -1 \leq x_t \leq 1; \quad 0 \leq a \leq 2; \quad (6)$$

and it shows different regimes according to the value of the control parameter  $a$  [5,33]. For small values of  $a$  the map is regular since it has non-positive Lyapunov exponents (see Fig.1). In particular, for  $a < \frac{3}{4}$  the iterates of the logistic map converge to a single fixed point  $x^* = f_a(x^*)$ , whose value depends on  $a$ . At  $a = \frac{3}{4}$  we have  $\lambda = 0$  and we observe the first pitchfork bifurcation: for a value slightly larger than  $\frac{3}{4}$  the iterates converge to a cycle-2. The number of points of the attractor  $f_a(x)$  keeps doubling at distinct, increasing values of the parameter  $a$ , until a critical value  $a_c = 1.401155198\dots$  is reached, where the attractor becomes infinite. This is known in the literature as the period-doubling route to chaos. In fact, beyond  $a_c$  the behavior of the logistic map is chaotic (positive Lyapunov exponent  $\lambda$ ) for most of the values of  $a$ . At the chaos threshold  $a = a_c$ ,  $\lambda$  is once again zero, and this point is the well known *edge of chaos* which has been the subject of intensive debates about the definition of what a complex systems is

<sup>1</sup> An equivalent, perhaps more popular version of the logistic map is  $x_{t+1} = rx_t(1-x_t)$ , with  $0 \leq x_t \leq 1$  and  $1 \leq r \leq 4$ . However, we notice that form (6) is easily generalized to other universality classes of order  $z \geq 1$ :  $x_{t+1} = 1 - a|x_t|^z$ . In this way, a  $z$ -logistic map is in fact representative of the universality class of unimodal maps of order  $z$ ; i.e., of one-dimensional maps with a single maximum of order  $z$ .

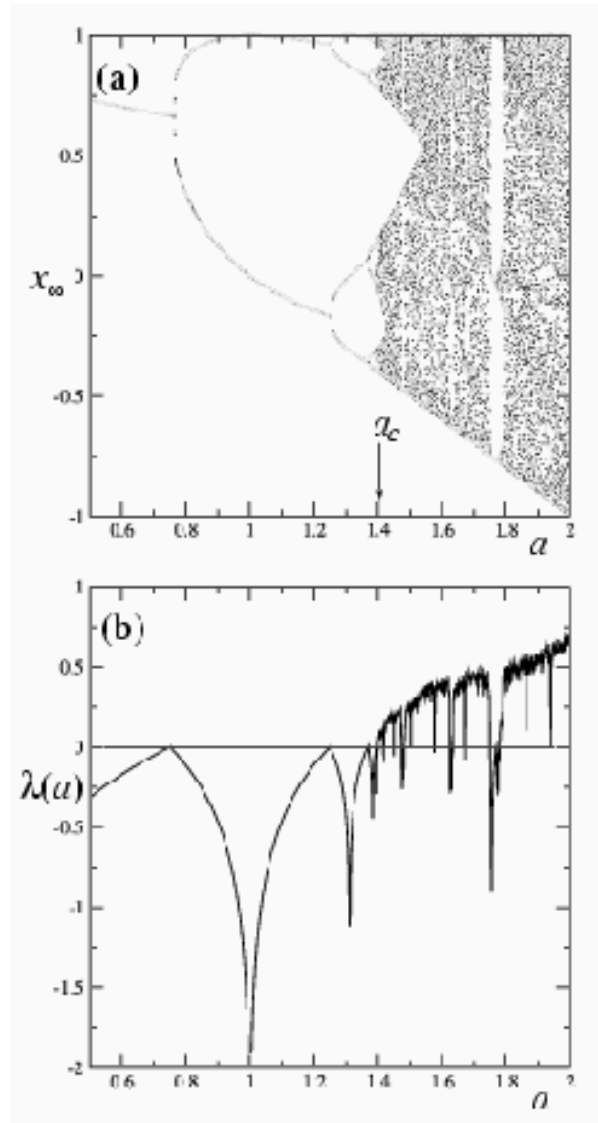


**Fig. 1.** (a) Attractor of the logistic map as a function of  $a$ . The edge of chaos is at the critical value  $a_c = 1.401155198\dots$  (b) Lyapunov exponent  $\lambda$  as a function of  $a$ .

[34,35]. It is exactly at the edge of chaos and at all other points where  $\lambda$  is zero (as at period doublings, but also for instance at inverse tangent bifurcations [5]), that a generalization of the standard BG entropy will be fruitful, as we show below.

**Sensitivity to initial conditions** Let us start by explaining better the meaning of the crucial concept of sensitivity to initial conditions. For all the cases in which the Lyapunov exponent  $\lambda$  is positive (negative) we expect on the average an exponential increase (decrease) of any small initial distance  $\xi(t) \equiv \frac{|\mathbf{x}_t - \mathbf{x}'_t|}{|\mathbf{x}_0 - \mathbf{x}'_0|}$  to hold. We typically have

$$\xi(t) = \exp(\lambda t), \quad (7)$$

where  $\mathbf{x}_t$  and  $\mathbf{x}'_t$  are the positions at time  $t$  of two initially close trajectories that may be considered, for the sake of generality, in a  $d$ -dimensional phase space. In the case of the logistic map  $d = 1$ . This case is referred in the literature as *strongly sensitive (insensitive)* to initial conditions. What is not usually reported in textbooks is what happens when  $\lambda$ , as defined by equation (7), is equal to zero. In Ref. [36] was proposed that in such situations the system still exhibits sensitivity to initial conditions, though in a form that is the  $q$ -generalization of Eq. (7):

$$\xi(t) = \exp_q(\lambda_q t) \equiv [1 + (1 - q)\lambda_q t]^{\frac{1}{1-q}} \quad (q \in \mathbb{R}). \quad (8)$$

This equation recovers Eq. (7) for  $q = 1$ , and displays a quite rich spectrum of possibilities according to the sign of  $\lambda_q$  and  $q$ . Let us concentrate on the case  $\lambda_q > 0$ ,  $q < 1$ . In this case the system presents a *weak sensitivity* to initial conditions, in the sense that two initially close trajectories diverge in time as a power-law instead than exponentially. A weakly sensitive system is well described once  $q$  and  $\lambda_q$  are given. In [36]  $q$  was calculated numerically for the logistic map at the edge of chaos, observing that the upper bound of  $\xi(t)$  lies on a line that is precisely a power-law (see Fig. 2); furthermore, it was conjectured that a value  $q = 0.2445\dots$  could be deduced from the Feigenbaum's constant  $\alpha$ . These results were recently confirmed in [37], where it was proved that, at the edge of chaos the upper bound of  $\xi(t)$  has exactly the form of Eq. (8), with  $q = 0.2445\dots$  and  $\lambda_q = \ln \alpha / \ln 2 = 1.3236\dots$ . In fact, as a consequence of the Feigenbaum's renormalization group recursion relation, two close initial conditions starting in the neighborhood of the origin  $x = 0$ , produce, each  $t = 2^n - 1$  ( $n = 0, 1, 2, \dots$ ), a dominant power-law separation of their iterates that has the form (8). After these particular steps, the iterates reproduce self-similar sequences, that are also power-laws. The effect of starting the initial points in other regions of the phase space instead that in the vicinity of  $x = 0$  is just a shifting in time of Fig. 2.

The renormalization group approach has proven powerful also at other points where the Lyapunov exponent is zero. In [38] the same  $q$ -exponential form (8) has been exactly obtained for the sensitivity to initial conditions at pitchfork and inverse tangent bifurcations, now with other values for  $q$  and  $\lambda_q$ . It is important to notice that the previous scheme of application of Eq. (8) generalizes to the other universality classes of unimodal maps of order<sup>2</sup>  $z > 1$ .

**Entropy production** The analysis of the entropy production provides an alternative approach to the same problem and a second way to characterize the

<sup>2</sup> See previous footnote.

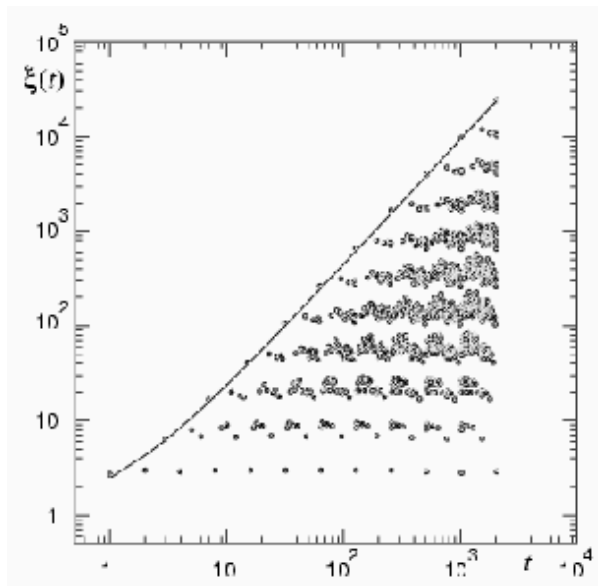


**Fig. 2.** Sensitivity to initial conditions for the logistic map at  $a = a_c$ . The dots represent  $\xi(t)$  for two initial data started at  $x_0 = 0$  and  $x'_0 \sim 10^{-8}$ . The solid line is the function in Eq. (8), with  $q = 0.2445\dots$  and  $\lambda_q = \ln \alpha / \ln 2 = 1.3236\dots$

$q$ -index at the edge of chaos. Instead of considering two trajectories initially close, we take a distribution of initial conditions localized in a tiny region of the phase space, we let this distribution evolve in time according to Eq. (6), and we study the increase of the entropy [39,6]. In the case of the logistic map, we can partition the phase space interval  $-1 \leq x \leq 1$  into  $W$  equal cells, and consider an initial distribution of  $N$  points placed at random inside one of the cells; the initial cell is also chosen randomly in the partition. The normalized number of points that occupy a cell defines a probability distribution:  $p_i \equiv n_i/N$  ( $\sum_{i=1}^W p_i = 1$ ), and as the system evolves, from the probabilities  $p_i(t)$  we can calculate the entropy production  $S_q(t)$ , via Eq. (1). In the chaotic regime the BG entropy ( $q = 1$ ) exhibits, before a saturation due to the finiteness of  $W$ , a linear increase in time, and in this stage the entropy production rate (that is expected to be equal to the Kolmogorov-Sinai entropy [40]) coincides with the positive Lyapunov exponent [41]. This is shown in Fig. 3 for the case  $a = 2$ , where  $S_q(t)$  is reported for three different values of  $q$ . As  $t$  evolves,  $S_q(t)$  increases (in all cases bounded by  $\frac{W^{1-q}-1}{1-q}$ , or  $\ln W$  when  $q = 1$ ), but only the curve for  $q = 1$  shows a clear linear behavior with a slope equal to the Lyapunov exponent  $\lambda = \ln 2$  [39]. For  $q < 1$  the curve is convex, while for  $q > 1$  the curve is concave. The slope in the linear stage does not depend on the dimension of the cells of the partition and on the size of the initial distribution. Therefore, in the chaotic regime the standard B-G entropy is the only  $q$ -entropy that displays a finite entropy production rate

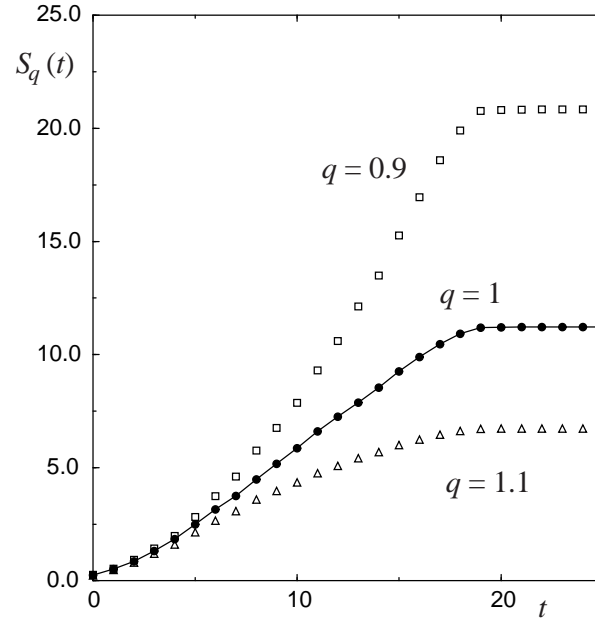


**Fig. 3.** Time evolution of  $S_q$  for the logistic map with  $a = 2$ . We consider three different values of  $q$ . The results are averages over 500 runs with  $N = 10^6$  and  $W = 10^5$ .

$\lim_{t \rightarrow \infty} \lim_{W \rightarrow \infty} S_q(t)/t$ . We wish now to repeat the same analysis at the edge of chaos, where  $\lambda$  is zero. Due to the power-law sensitivity to initial conditions and to the fractality of phase space (the attractor now is a multifractal) we expect that anomalous behavior may be observed. In Fig. 4 we consider  $a = a_c$  and we plot  $S_q(t)$  for four different values of  $q$ ; the curves are obtained with a large  $W$  and with an average over many different runs since the complexity of the phase space originates many fluctuations. Consistently with the value of  $q$  extracted for the sensibility to initial conditions, the result is that the growth of  $S_q(t)$  is found to be linear when  $q = 0.2445\dots$ , while for  $q < q_c$  ( $q > q_c$ ) the curve is convex (concave). This behavior is similar to the one of Fig. 3, with a major difference: the linear growth is not at  $q = 1$ , but at  $q = 0.2445\dots$  [6].

**Multifractal analysis** There is also a third, geometrical method that allows us to calculate the  $q$  of the logistic map. This method is based only on the description of the multifractal attractor existing at  $a = a_c$ , and gives exactly the same value we have already obtained. The multifractal attractor can be characterized by using the multifractal function  $f(\alpha)$  [33]. This function is defined in the interval  $[\alpha_{min}, \alpha_{max}]$ , and its maximum equals the fractal or Hausdorff

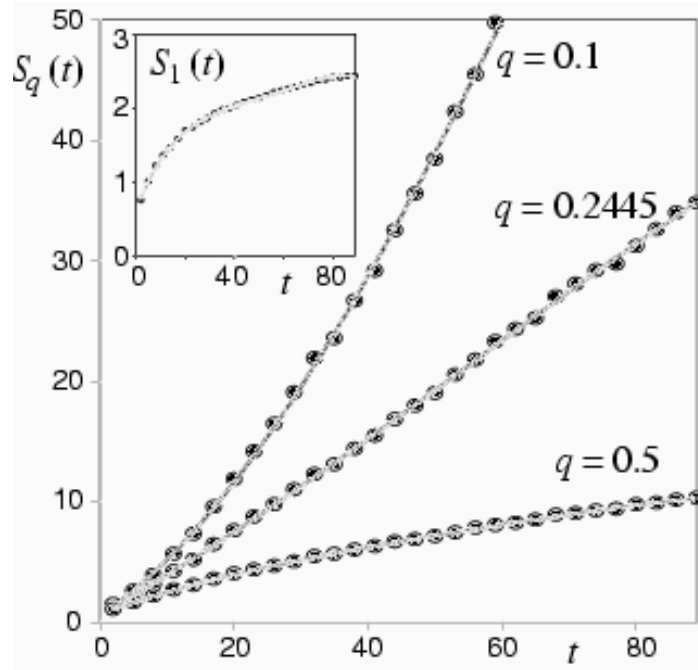


**Fig. 4.** Time evolution of  $S_q$  for the logistic map with  $a = a_c$ . We consider four different values of  $q$ . The case  $q = 1$  is in the inset.  $W = N = 2.5 \cdot 10^6$  and results are averages over 15115 runs.

dimension  $d_f$ . The value of  $q$  can be calculated from [36]:

$$\frac{1}{1-q} = \frac{1}{\alpha_{min}} - \frac{1}{\alpha_{max}}, \quad (9)$$

where  $\alpha_{min}$  ( $\alpha_{max}$ ) are the two values for which  $f(\alpha)$  is defined. In particular for the logistic map at the edge of chaos  $\alpha_{min} = 0.380\dots$ ,  $\alpha_{max} = 0.755\dots$  and we have again  $q = 0.2445\dots$

### 3.2 Conservative Maps: the standard map

Conservative systems present quite different statistical properties than dissipative ones. One of these differences is that the transition from chaoticity to regularity happens in the phase space without an ‘edge of chaos’, but in a rather complicated way as described by the Kolmogorov-Arnold-Moser (KAM) theorem [42], see Fig. 5e-g). Conservative maps may be derived, for example, from Hamiltonian systems. In this case the original system is characterized by an even number of dimensions  $d = 2n$ , where  $n$  is the number of degrees of freedom. If the Hamiltonian  $H$  is time-independent the dimension can be reduced by one.

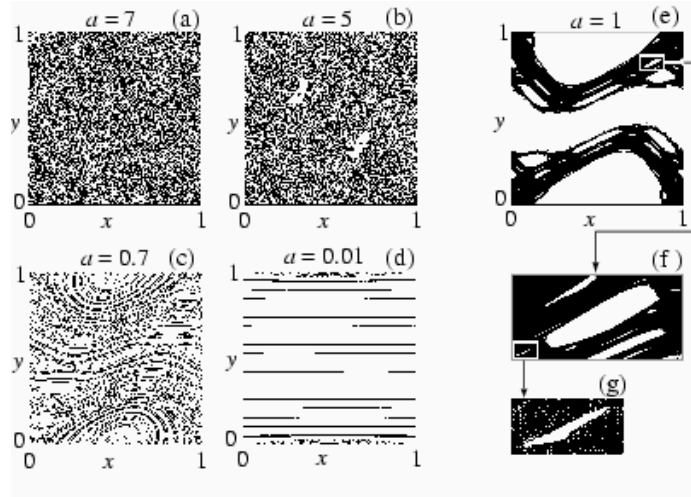


**Fig. 5.** (a)–(d) Phase portrait of the standard map for typical values of  $a$ .  $N = 20 \times 20$  orbits (black dots) were started with a uniform distribution in the unit square and traced for  $0 \leq t \leq 200$ . (e)–(g) Islands-around-islands. (e):  $N = 100 \times 100$  initial data were started inside a small square of side  $\sim 10^{-2}$  and traced for  $0 \leq t \leq 5000$ . (f) is a magnification of the island inside the rectangle in (e). (g) is a magnification of the island inside the rectangle in (f).

Moreover, as in statistical mechanics we are interested mostly in *recurrent trajectories* (i.e., in those trajectories that come back again and again, indefinitely, to any part of the phase space they have once visited), we can take a *Poincaré section* of the phase space cutting transversally the constant-energy hypersurface and considering the successive intersections of each orbit with this transversal surface. In this way we reduce the dimension of the phase space to  $d_M = 2n - 2$  and we obtain a great numerical simplification, as we can now analyze a discrete-time iteration map instead of a continuous-time system of differential equations. The map thus obtained may be shown to be *symplectic* (see, e.g. [42]); this implies that the  $d_M$  Lyapunov exponents are coupled in pairs, where each member of the pair has the opposite of the other.

The minimum dimension that allows for the application of this scheme is  $d_M = 2$  ( $n = 4$ ), and a paradigmatic example of this kind, that plays for conservative systems a similar role the logistic map plays for dissipative ones, is the standard map, that may be characterized by the equations<sup>3</sup>:

$$\begin{aligned}
 x_{t+1} &= y_t + \frac{a}{2\pi} \sin(2\pi x_t) + x_t \pmod{1}, \\
 y_{t+1} &= y_t + \frac{a}{2\pi} \sin(2\pi x_t) \pmod{1},
 \end{aligned}
 \tag{10}$$

<sup>3</sup> The map is also known as the kicked rotator map.

where  $a \in \mathbb{R}$  ( $t = 0, 1, \dots$ ). The system is integrable when  $a = 0$ , while, roughly speaking, chaoticity increases when  $|a|$  increases (see Fig. 5a-d).

As for the logistic map, we expect that anomalous effects may be produced as the complexity of the phase space increases (i.e., when we pass from the chaotic to the regular regime reducing  $|a|$ ), and as this happens, we would like to see how the nonextensive formalism generalizes the BG one, at least for some of the statistical variables we have previously described.

**Sensitivity to initial conditions** In the case of the standard map, the sensitivity to initial condition depends dramatically on the position in the phase space. Chaotic regions produces exponential separation of initially close trajectories, while regular regions exhibit linear separation of initially close orbits. At the border between these regions, appear fractal-like structures of islands-around-islands (see, e.g., [43], see Fig. 5e-g). We notice however that in statistical mechanics we are mainly interested in extracting global averages behaviors, so that we can try to calculate an average  $\xi(t)$  by sampling uniformly the whole phase space. When this experiment is performed for rather small values of  $|a|$ , as we show in Fig. 6, a *crossover* in time between two different regimes occur [44]. Fig. 6a displays in fact a linear increase of  $\ln(\xi(t))$  only after a certain iteration step. Correspondingly, Fig. 6b exhibits a linear increase of  $\ln_q(\xi(t))$  precisely for those steps where  $\ln(\xi(t))$  is concave (numerically it was found  $q \simeq 0.3$ ). Moreover, the crossover time increases when  $|a|$  decreases. This means that two different behaviors dominates the average sensitivity to initial conditions for different time. Initially, because of the predominance of fractal-like structures in the phase space, the sensitivity to initial conditions is power-law; then, after a certain time, the sensitivity to initial conditions becomes exponential due to the rapidity of the exponential growth if compared with the power-law. If we wish to model such a behavior with a single function, we can first observe that exponential and power-law sensitivity to initial conditions may be viewed as solution of the differential equations  $\dot{\xi} = \lambda\xi$  and  $\dot{\xi} = \lambda_q\xi^q$  respectively. A differential equation describing a crossover in time is then:  $\dot{\xi} = \lambda\xi + (\lambda_q - \lambda)\xi^q$  ( $q < 1$ ,  $\lambda, \lambda_q > 0$ ). The solution [45]

$$\xi(t) = \left[ 1 - \frac{\lambda_q}{\lambda} + \frac{\lambda_q}{\lambda} e^{(1-q)\lambda t} \right]^{\frac{1}{1-q}}, \quad (11)$$

presents, in the case  $0 < \lambda \ll \lambda_q$ , three asymptotic behaviors, namely (i) linear:  $\xi \sim 1 + \lambda_q t$ , for  $0 \leq t \ll t_{cross1} \equiv \frac{1}{(1-q)\lambda_q}$ ; (ii) power-law:  $\xi \sim [(1-q)\lambda_q]^{\frac{1}{1-q}} t^{\frac{1}{1-q}}$ , for  $t_{cross1} \ll t \ll t_{cross2} \equiv \frac{1}{(1-q)\lambda}$ ; (iii) exponential:  $\xi \sim \left(\frac{\lambda_q}{\lambda}\right)^{\frac{1}{1-q}} e^{\lambda t}$ , for  $t \gg t_{cross2}$ .

**Entropy production** If the connection between sensitivity to initial condition and entropy production that we have observed for the logistic map is correct, we should observe a crossover between different statistical regimes even when we analyze the entropy production of the standard map. This has been done

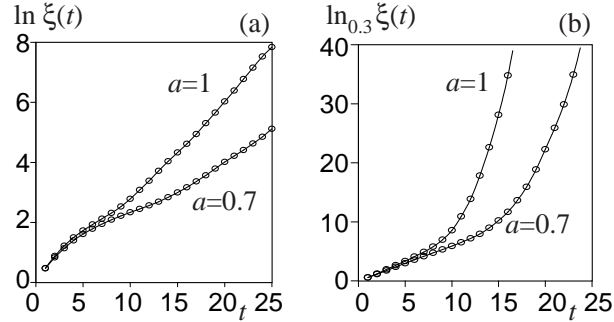


**Fig. 6.** Average sensitivity to initial conditions of the standard map for small values of  $a$ .  $|\mathbf{x}_0 - \mathbf{x}'_0| \sim 10^{-9}$  and results are averages over 5000 runs. An initial separation of order  $\ln$  (a)  $\ln(\xi(t))$  displays a linear increase only after a certain time. Correspondingly, in (b)  $\ln_{0.3}(\xi(t))$  exhibits a linear increase for the initial steps.

in [46], with a numerical experiment analogous to the one previously described for the logistic map and that is difficult to perform because of the complexity of the phase space and the related effects of rapid saturation of the entropy for  $W$  finite. In Figs. 7 and 8 we display how, for small values of  $|a|$  and before saturation begins, the entropy production of  $S_1(t)$  becomes linear only after a stage where  $S_q(t)$  is linear, with, once again, a value  $q \simeq 0.3$ . Notice that the crossover time tends to infinity when  $|a|$  goes to zero, so that in this limit the stage characterized by the power-law sensitivity to initial conditions and by this nonstandard entropy production lasts for infinite time.

## 4 Applications to Many-particle systems

### 4.1 Hamiltonian nonextensive systems: the HMF model

In the last years there has been an intense research activity in investigating microscopic dynamical features in connection with macroscopic features. In particular several authors have focused their attention in characterizing from a dynamical point of view macroscopic phase transitions [47,48,49,50,51]. It has been found, for example, that in correspondence of a phase transition there is a peak in the chaoticity of the microscopic dynamics. In general chaoticity is of fundamental importance for any system to reach the standard equilibration. Anomalies should be expected when this does not occur, since ergodicity breaking might happen and the system can remain trapped in some region of phase space. In this respect a model whose features have been particularly interesting is the Hamiltonian Mean Field model, from here on referred as HMF model, and its generalizations where the range of the interaction can be changed. The model was introduced in ref [8] and extensively studied in refs [8,9,10,11,13,14]. In this volume one chapter is dedicated to its equilibrium properties both from a dynamical and from a thermodynamical point of view [12]. In the present

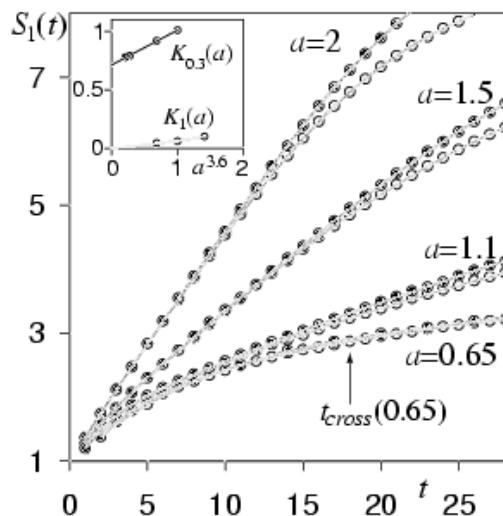


**Fig. 7.** For the standard map we show  $S_1(t)$  for different values of  $a \leq 2$  (5000 to 7000 runs were averaged). Full circles correspond to  $N = W = 1000 \times 1000$  for  $a = 2, 1.5, 1.1$  ( $N = W = 5000 \times 5000$  for  $a = 0.65$ ); empty circles correspond to  $N = W = 448 \times 448$  for  $a = 2, 1.5, 1.1$  ( $N = W = 2236 \times 2236$  for  $a = 0.65$ ). Inset: Slopes of  $S_1(t)$  ( $K_1(a)$ ) and of  $S_{0.3}(t) = 20$  ( $K_{0.3} \simeq 0.71 + 0.30 a^{3.6}$ ) in their linear regimes (see also Fig. 8). The lines are guides to the eye.

section we consider only the anomalies found in the out-of-equilibrium regime before equilibration to the Boltzmann-Gibbs regime and how these behavior can be related to nonextensive statistics [29].

The HMF model describes a system of  $N$  planar classical spins interacting through an infinite-range potential[8]. The Hamiltonian can be written as:

$$H = K + V = \sum_{i=1}^N \frac{p_i^2}{2} + \frac{1}{2N} \sum_{i,j=1}^N [1 - \cos(\theta_i - \theta_j)] \quad , \quad (12)$$

where  $\theta_i$  is the  $i$ th angle and  $p_i$  the conjugate variable representing the angular momentum or the rotational velocity since unit mass is assumed. The interaction is the same as in the ferromagnetic XY model [3], though the summation is extended to all couples of spins and not restricted to first neighbors. Following the Kac procedure [12], the coupling constant in the potential is divided by  $N$ . This makes  $H$  only formally extensive ( $V \sim N$  when  $N \rightarrow \infty$ )[29,15,13,14], since the energy remains non-additive, i.e. the system cannot be trivially divided in two independent sub-systems. The canonical analytical solution of the model predicts a second-order phase transition. At low energy density the system is in a ferromagnetic phase characterized by a magnetization  $M \sim 1$ , where  $M$  is the

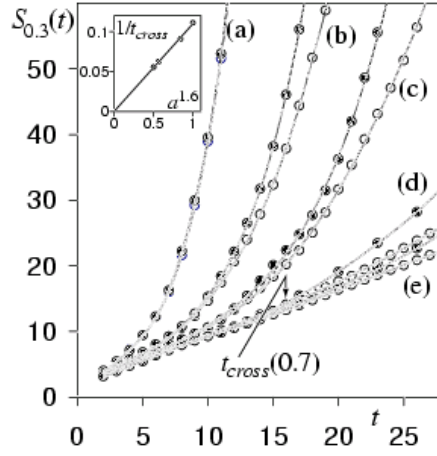


**Fig. 8.** For the standard map we show  $S_{0.3}(t)$  for:  $a = 1.5$  (a);  $a = 1.1$  (b);  $a = 0.9$  (c);  $a = 0.7$  (d);  $a = 0.65$  (e) (5000 to 7000 runs were averaged). Full circles correspond to  $N = W = 1000 \times 1000$  for (a), (b), (c),  $N = W = 5000 \times 5000$  for (d), (e); empty circles correspond to  $N = W = 448 \times 448$  for (a), (b), (c),  $N = W = 2236 \times 2236$  for (d), (e). Inset:  $t_{cross}(a)$  defined as the intersection of the linear part (before it starts bending) and a standard extrapolation of the bended part of the curves  $S_{0.3}(t)$ . Notice that  $t_{cross}(a)$  diverges for  $a \rightarrow 0$ . The lines are guides to the eye. Our results suggest  $\lim_{t \rightarrow \infty} \lim_{a \rightarrow 0} \lim_{W \rightarrow \infty} \lim_{N \rightarrow \infty} \frac{S_{0.3}(t)}{t} \simeq 0.71$  for  $q = q^* \simeq 0.3$ , whereas this limit vanishes (diverges) for  $q > q^*$  ( $q < q^*$ ).

modulus of

$$\mathbf{M} = \frac{1}{N} \sum_{i=1}^N \mathbf{m}_i, \quad (13)$$

with  $\mathbf{m}_i = [\cos(\theta_i), \sin(\theta_i)]$ . Increasing the energy beyond a critical value, the spins become homogeneously oriented on the unit circle and  $M \sim 0$ . The *caloric curve*, i.e. the dependence of the energy density  $U = E/N$  on the temperature  $T$ , is given by  $U = \frac{T}{2} + \frac{1}{2}(1 - M^2)$  [12] and shown in Fig.9 as a full curve. The critical point is at energy density  $U_c = 0.75$  corresponding to a critical temperature  $T_c = 0.5$  [8]. The dynamical behavior of HMF can be investigated in the micro-canonical ensemble by starting the system with water bag initial conditions, i.e.  $\theta_i = 0$  for all  $i$  ( $M = 1$ ) and velocities uniformly distributed, and integrating numerically the equations of motion [9]. As shown in Fig.9, microcanonical simulations are in general in good agreement with the canonical ensemble, except for a region below  $U_c$ , where it has also been found a dynamics characterized by Lévy walks, anomalous diffusion [10] and a negative specific heat[11]. Ensemble inequivalence and negative specific heat have also been found in self-gravitating systems [52], nuclei and atomic clusters [53,54,55,56]. In our case such anomalies emerge as dynamical transient features, although in a generalized version of the HMF model [51,12] it seems that they remain also in the BG equilibrium

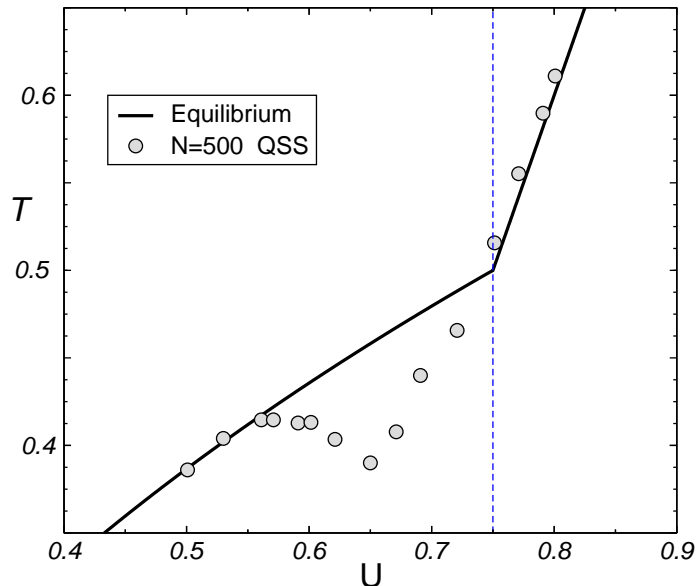


**Fig. 9.** We compare the equilibrium caloric curve of the HMF model (full curve) with the numerical simulation for a system of size  $N=500$ . The numerical integration is followed up to a short time, when the system is in the metastable quasi-stationary state (QSS).

regime. In order to understand better this disagreement we focus on a particular energy value, namely  $U = 0.69$  below the critical energy, and we study the time evolution of temperature, magnetization, and velocity distributions.

In Fig.10 we report the temporal evolution of  $2 \langle K \rangle / N$  for  $U = 0.69$  and  $N = 500$ . This quantity, at equilibrium, is expected to coincide with the temperature ( $\langle \cdot \rangle$  denotes time averages). The figure shows that when the system is started with out-of-equilibrium initial conditions (water bag in our case) rapidly reaches a metastable quasi-stationary state (QSS) which does not coincide with the canonical prediction. After a short transient time, not reported here,  $2 \langle K \rangle / N$  shows a plateau corresponding to a  $N$ -dependent temperature  $T_{QSS}(N)$  (and  $M_{QSS} \sim 0$ ,  $M \rightarrow 0$  if  $N \rightarrow \infty$ ) lower than the canonical temperature. This metastable state needs a long time to relax to the canonical equilibrium state with temperature  $T_{can} = 0.476$  and magnetization  $M_{can} = 0.307$ . In the same figure we plot a typical single-particle motion in the two insets. In panel (b) the motion is characterized by anomalous diffusion and Lévy walks with constant velocity[10]. This motion is well described by a model introduced in ref. [57]. These features change at equilibration, see panel (c) where the motion is a standard random walk and diffusion becomes normal. In ref. [10] it has been found that the lifetime of the metastable QSS and the crossover time from anomalous to normal diffusion do coincide within the numerical accuracy

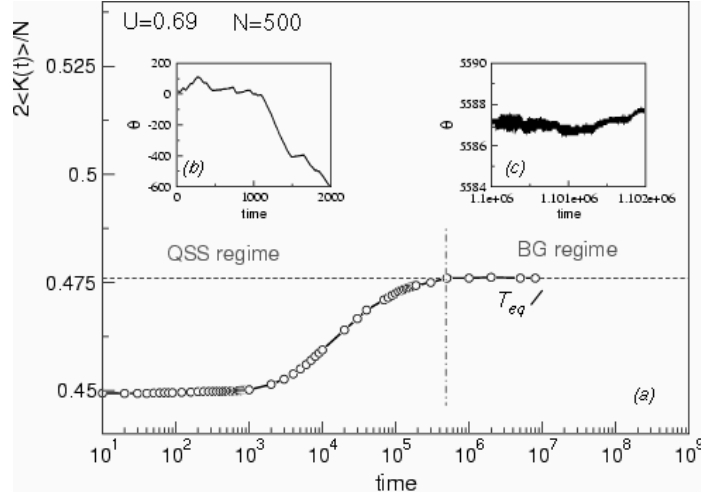


**Fig. 10.** For the HMF model at  $U=0.69$  and  $N=500$ , we plot the temperature, calculated by means of the average kinetic energy, as a function of time. Two plateaux emerge from the calculation. The first one is the metastable quasi-stationary state (QSS), while the second one corresponds to the Boltzmann-Gibbs (BG) equilibrium regime. In the inset (b) we show the angle vs time of a typical rotor in the metastable regime: the motion shows Lévy walks and anomalous diffusion [10]. In the inset (c) we show the single-particle motion in the BG equilibrium regime: the motion is a random walk.

adopted. On the other hand, the duration of the plateau increases with the size of the system. In fact the lifetime of QSS has a linear dependence on  $N$  as shown in Fig.11 where simulations for different out-of-equilibrium initial conditions are plotted. These numerical results indicate that the two limits  $t \rightarrow \infty$  and  $N \rightarrow \infty$  do not commute: if the thermodynamic limit is performed before the infinite time limit, the system does not relax to the BG equilibrium and the anomalies discussed above remain forever. Indeed similar features have also been found for spin glasses[58,59] and granular matter [64,60] and could probably be interpreted within a general theoretical scenario. When  $N$  increases  $T_{QSS}(N)$  tends to a definite value which is  $T_\infty = 0.38$ . The latter is obtained analytically as the metastable prolongation, at energies just below  $U_c = 0.75$ , of the high-energy branch characterized by  $M = 0$ . In ref.[61] we have also found that  $[T_{QSS}(N) - T_\infty] \propto N^{-1/3}$ . This scaling, exploiting the expression for the caloric curves, implies also a scaling of the magnetization, which goes to zero like  $M_{QSS} \propto N^{-1/6}$ . A further numerical check of this law was obtained in ref.[62].

It is important at this point to discuss the behavior of the Lyapunov exponents as a function of  $N$  and of time in order to investigate if also this measure shows some anomaly. In fact this is just the case: also the largest Lyapunov exponent  $\lambda$  has two temporal regimes and in particular two plateaux. We plot in Fig.12 the time evolution of  $\lambda$  for the case  $U = 0.69$  and  $N = 500$ . The nu-

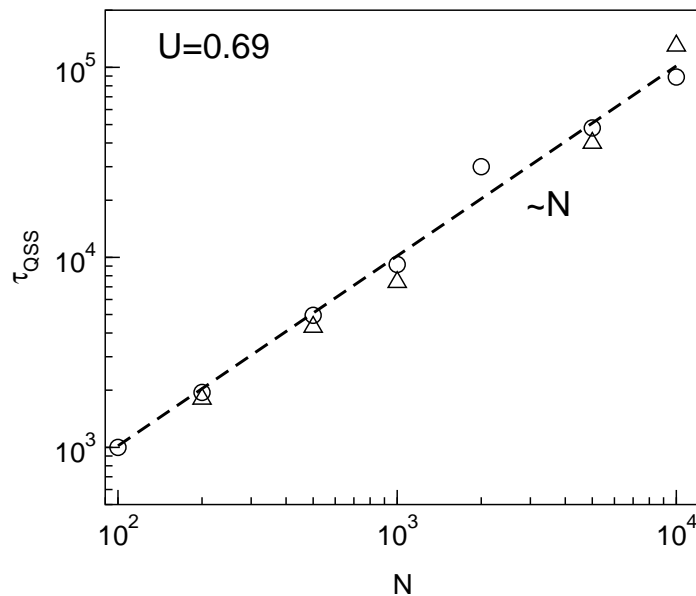


**Fig. 11.** For the HMF model we plot the lifetime of the metastable quasi-stationary state,  $\tau_{QSS}$ , for  $U=0.69$ , as a function of  $N$ . Different out-of-equilibrium initial conditions are indicated by different symbols. The figure shows that the duration of these states diverges with  $N$ .

merical simulation averaged over 350 events shows that in the metastable QSS regime the largest Lyapunov exponent is smaller than at the BG equilibrium. In the inset we report the scaling of  $\lambda$  in the QSS regime as a function of the size: increasing  $N$ ,  $\lambda_{QSS}$  tends to zero as  $N^{-1/9}$  [62]. The scaling law for the Lyapunov exponent can be related to the scaling of the magnetization as discussed in ref.[62]. The fact that  $\lambda \rightarrow 0$  for  $N \rightarrow \infty$  implies that mixing is negligible as  $N$  increases and one expects anomalies in the relaxation process in the sense advanced by Krylov [63] and in a very similar way to the case of the maps discussed in the previous section.

In order to check relaxation in HMF not only the temperature, the second moment, but also the higher moments of the velocity distribution should coincide with those of the BG equilibrium one. In Fig.13 we focus our attention on the velocity probability distribution functions (pdfs). The figure shows that the initial uniform velocity pdfs, quickly acquire and maintain for the complete duration of the metastable state a *non-Gaussian shape*. In particular the velocity pdf of the QSS is wider than a Gaussian (drawn as dashed curve) for small velocities, but shows a faster decrease for  $p > 1.2$ . The enhancement for velocities around  $p \sim 1$  is consistent with the anomalous diffusion and the Lévy walks (with average velocity  $p \sim 1$ ) observed in the QSS regime [10]. The following rapid decrease for  $p > 1.2$  is due to conservation of total energy. The stability of the QSS velocity

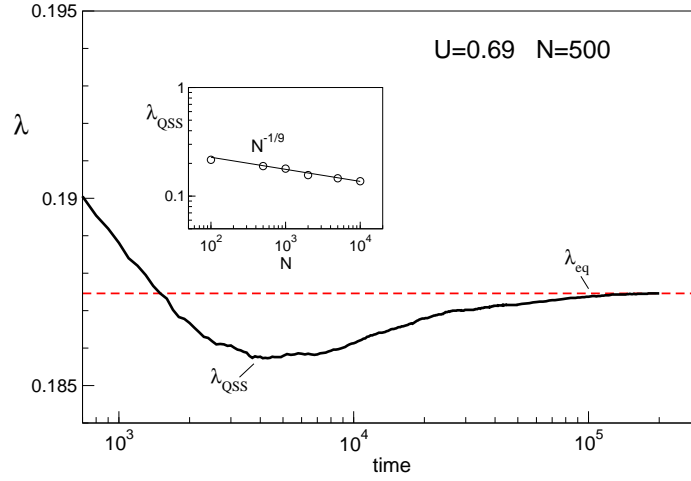


**Fig. 12.** We plot the largest Lyapunov exponent,  $\lambda$ , vs time for the HMF model at  $U = 0.69$  and  $N = 500$ . Two plateaux are found also in this case. In the inset we show that  $\lambda_{QSS}$  goes to zero as  $N^{-1/9}$ . This behavior can be explained with the anomalous fluctuations of the magnetization. See text for further details.

pdf can be explained by the fact that, since for  $N \rightarrow \infty$ ,  $M_{QSS} \rightarrow 0$  also the force on the spins tends to zero with  $N$ , being  $F_i = -M_x \sin \theta_i + M_y \cos \theta_i$ . If  $N$  is finite, one has only a small random force, which makes the system eventually evolve into the usual Maxwell-Boltzmann distribution after some time. When this happens, Lévy walks disappear and anomalous diffusion leaves place to Brownian diffusion[10], see insets in Fig.10. Nonextensive thermodynamics is able to reproduce the non-Gaussian pdf reported in Fig.13. In fact the nonextensive formalism provides, for the canonical ensemble, a  $q$ -dependent power-law distribution in the variables  $p_i$ ,  $\theta_i$ . This distribution has to be integrated over all  $\theta_i$  and all but one  $p_i$  in order to obtain the one-momentum pdf,  $P_q(p)$ , to be compared with the numerical one,  $P_{num}(p)$ , obtained by considering, within the present molecular dynamical frame, increasingly large  $N$ -sized subsystems of an increasingly large  $M$ -system. Within the  $M \gg N \gg 1$  numerical limit, we expect to go from the microcanonical ensemble to the canonical one (the cut-off is then expected to gradually disappear as indeed occurs in the usual short-range Hamiltonians), thus justifying the comparison between  $P_q(p)$  and  $P_{num}(p)$ . The enormous complexity of this procedure made us to turn instead onto a naive, but tractable, comparison, namely that of our present numerical results with the following one-free-particle pdf [29,15]  $P(p) \propto [1 - (\frac{1}{2T})(1-q)p^2]^{1/(1-q)}$ , which recovers the Maxwell-Boltzmann distribution for  $q = 1$ . The same type of formula has been recently used to describe successfully turbulent Couette-Taylor flow [16] and non-Gaussian pdfs related to anomalous diffusion of *Hydra* cells in cellular aggregates. In the case of HMF the best fit is obtained by a curve with entropic index  $q = 7$ , and temperature  $T = 0.38$ . The agreement between

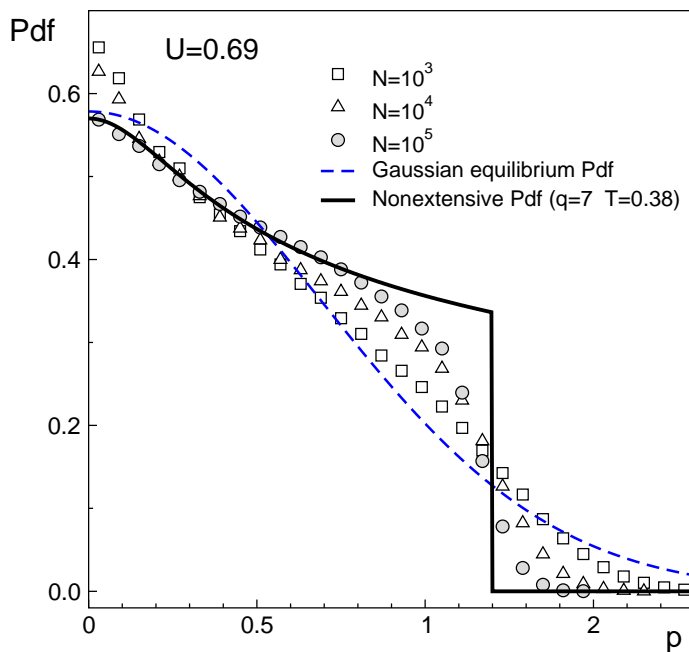


**Fig. 13.** We plot the velocity probability distribution functions of the HMF model for  $U=0.69$  and different  $N$  values (open symbols). The Gaussian equilibrium shape is also plotted (dashed curve) together with the fit with the nonextensive pdf formula obtained for  $q = 7$  and  $T = 0.38$  (full curve).

numerical results and theoretical curve improves with the size of the system. A finite-size scaling confirming the validity of the fit was reported in ref. [61]. Since in our case we get  $q > 3$ , the theoretical curve does not have a finite integral and thus it needs to be truncated with a sharp cut-off in order to make the total probability equal to one. It is however clear that, the fitting value  $q = 7$  is only an effective nonextensive entropic index. In ref.[61] we verified, through the calculation of the fractal dimension  $D_2$ , that a dynamical correlation emerges in the  $\mu$ -space before the final arrival to a quasi-uniform distribution. During intermediate times some filamentary structures appear, a similar feature has recently been found also in self-gravitating systems[50], which might be closely related to the plateaux observed in Fig.10. We have found that these correlations do not sensibly depend on  $N$ , thus likely the possible connection does not concern the entire  $\mu$ -space, but perhaps only the small sticky regions between the "chaotic sea" and the quasi-orbits[65]. Recently another application of the generalized nonextensive formalism has been observed for this model in the relaxation regime. It has been found that the time relaxation of macroscopic quantities, like the temperature for example, obey power-laws and more specifically  $q$ -exponential curves. To illustrate this, in Fig.14, we plot the time relaxation of the temperature to its final value for  $U = 0.69$  and for two sizes  $N=500,1000$ . In particular we show

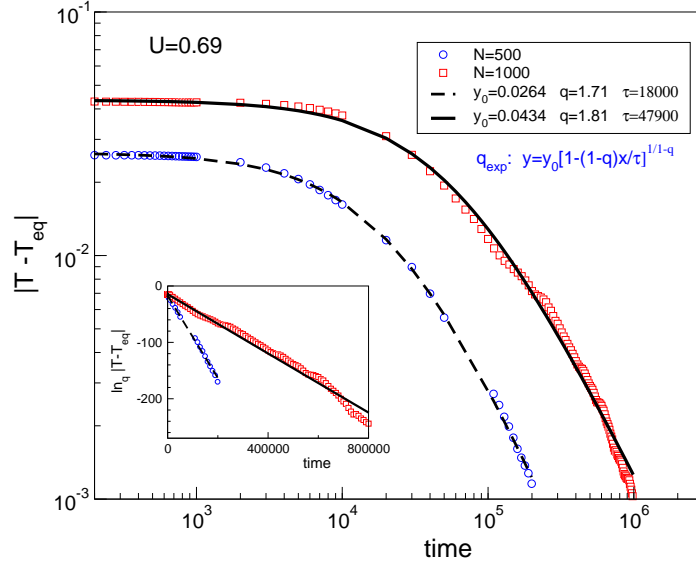


**Fig. 14.** For the HMF model, we plot the difference between the temperature  $T$  and that one at equilibrium  $T_{eq}$ , for  $U=0.69$  and  $N=500,1000$ , vs time (open symbols). The points are the result of an ensemble average over 1000 runs. The figure shows that the relaxation process is a power law in time and can be very well reproduced with a decreasing  $q$ -exponential. We report the  $q$ -exponential fits for comparison (full and dashed curves). In the inset we plot the  $q$ -logarithm of the same data. The entropic index  $q$  is related to relaxation and should not necessarily be equal to that one of velocity pdfs.

$y(t) = |T - T_{eq}|$ , with  $T_{eq} = 0.476$  as a function of the time  $t$ . The system relaxes to equilibrium according to the  $q$ -exponential formula<sup>4</sup>

$$y(t) = y_0 \left[ 1 - (1 - q) \frac{t}{\tau} \right]^{1/(1-q)}, \quad (14)$$

where  $q$  is the entropic index,  $\tau$  a characteristic time and  $y_0$  a saturation value [29]. For  $N = 500$  the same data shown in Fig.10 are used. For this particular size, one finds a value of the entropic index equal to  $q = 1.71$  and a characteristic relaxation time  $\tau = 18000$ . A slightly greater value of  $q$  equal to 1.81 is found for  $N=1000$ . In the inset we report the  $q$ -logarithm of same data [66]. This entropic index  $q$  is related to the relaxation and there is no reason to be exactly the same as the one obtained for the velocity pdfs. It is interesting to notice that similar relaxation process characterized by a  $q$ -exponential has been recently discovered also in echo experiment on the Internet [67]. Two final considerations before concluding this section. The first one is that in ref.[68] it has been found that

<sup>4</sup> The minus in front of the term  $(1 - q)$  at variance with formula (4) is due to the fact we are considering a decreasing  $q$ -exponential and  $q > 1$ .

the HMF model shows aging in correspondence of the metastable QSS. Thus it is a very intriguing challenge left for future investigation, the study of the possible connections between spin glasses, hamiltonian mean field models and nonextensive statistics. Second, the anomalies we have found are not a peculiar characteristic of the HMF model. In fact the same behavior has been found also in a generalization of the HMF model, the  $\alpha - XY$  model [13,14], in which the spins are placed on a  $d$ -dimensional lattice, and the interaction energy between two generic spins  $i$  and  $j$  (of formula (12)) is modulated by an extra factor  $1/r_{ij}^\alpha$ . Here  $r_{ij}$  is the distance between spin  $i$  and spin  $j$  [14]. If  $\alpha/d < 1$  nonextensivity induces anomalies similar to those described for the HMF model. Conversely, if  $\alpha/d > 1$ , i.e. when the potential decreases rapidly enough with  $r$ , the  $\alpha - XY$  model behaves in the standard way and does not exhibit any of the anomalies discussed in this section. Similar features induced by nonextensivity have been found also for long-range Lennard-Jones-like potentials [69].

## 5 Conclusions

We have finally ended our guided tour in the realm of nonextensive systems. Our choice was to focus only on a few simple examples, chosen in order to represent the most instructive classes of systems. On one hand we have considered *low-dimensional systems*, in particular low-dimensional maps as the logistic map (representative of a dissipative system), and the standard map (representative of conservative systems). On the other hand we have considered *high-dimensional systems* discussing the anomalies observed in the HMF model, a classical many-body long-range-interacting Hamiltonian. Though representing very different kind of systems, all the examples reported share some common properties: long-range correlations in space/time, either long-range microscopic interactions or long-range microscopic memory (nonmarkovian processes), or (multi)fractal boundary conditions, or, generically speaking, some mechanism which creates a scale-invariant hierarchical structure of some sort. Such properties appear in classical many-body Hamiltonians and low-dimensional nonlinear dynamical systems everytime that the Lyapunov exponents approach zero, i.e. when chaos (strong mixing) is impossible and the sensitivity to the initial conditions is not exponential in time. In most cases of weak sensitivity to initial conditions, a generalized nonextensive formalism may replace standard thermostatics.

## References

1. F. Takens, in *Structures and Dynamics - Finite Dimensional Deterministic Studies*, eds. H.W. Broer, F. Dumortier, S.J. van Strien and F. Takens (North Holland, Amsterdam, 1991), p. 253; A.C.D. van Enter, R. Fernandez and A.D. Sokal, J. Stat. Phys. **72**, 879 (1993).
2. A. Einstein, Annalen der Physik **33** (1910) 1275. E.G.D. Cohen, Physica A **305**, 19 (2002); M. Baranger, Physica A **305**, 27 (2002); C. Beck and E.G.D. Cohen, [cond-mat/0205097].

3. L. Tisza, *Generalized Thermodynamics*, MIT Press (1966); P.T. Landsberg, *Thermodynamics and Statistical Mechanics*, Dover (1991).
4. D.H.E. Gross, *Thermo-Statistics or Topology of the Microcanonical Entropy Surface*, in this volume.
5. H.G. Schuster, *Deterministic Chaos. An Introduction*, 3rd Revised Edition (VCH Publishers, Weinheim, 1995).
6. V. Latora, M. Baranger, A. Rapisarda, C. Tsallis, Phys. Lett. A **273**, 97 (2000); M. Baranger, V. Latora, and A. Rapisarda, Chaos Solitons and Fractals **13**, 471 (2001); U. Tirnakli, Physica A **305**, 119 (2002).
7. M. Tabor, *Chaos and Integrability in Nonlinear Dynamics*, Wiley, New York (1989).
8. M. Antoni and S. Ruffo, Phys. Rev. E **52**, 2361 (1995).
9. V. Latora, A. Rapisarda and S. Ruffo, Phys. Rev. Lett. **80**, 692 (1998); Physica D **131**, 38 (1999) and Progr. Theor. Phys. Suppl. **139**, 204 (2000).
10. V. Latora, A. Rapisarda and S. Ruffo, Phys. Rev. Lett. **83**, 2104 (1999) and Physica A **280**, 81 (2000).
11. V. Latora and A. Rapisarda, Nucl. Phys. A **681**, 331c (2001).
12. T. Dauxois, V. Latora, A. Rapisarda, S. Ruffo and A. Torcini, *The Hamiltonian Mean Field Model: from Dynamics to Statistical Mechanics and Back*, in this volume.
13. C. Anteneodo and C. Tsallis, Phys. Rev. Lett. **80**, 5313 (1998); F. Tamarit and C. Anteneodo, Phys. Rev. Lett. **84**, 208 (2000).
14. A. Campa, A. Giansanti and D. Moroni, Phys. Rev. E **62**, 303 (2000) and Physica A **305**, 137 (2002).
15. C. Tsallis, in *Nonextensive Statistical Mechanics and Thermodynamics*, eds. S.R.A. Salinas and C. Tsallis, Braz. J. Phys. **29**, 1 (1999); in *Nonextensive Statistical Mechanics and Its Applications*, eds. S. Abe and Y. Okamoto, Series Lecture Notes in Physics (Springer-Verlag, Heidelberg, 2001); , in *Classical and Quantum Complexity and Nonextensive Thermodynamics*, eds. P. Grigolini, C. Tsallis and B.J. West, Chaos, Solitons and Fractals **13**, Number 3, 371 (Pergamon-Elsevier, Amsterdam, 2002); in *Non Extensive Statistical Mechanics and Physical Applications*, eds. G. Kaniadakis, M. Lissia and A. Rapisarda, Physica A **305**, 1 (2002); in *Nonextensive Entropy - Interdisciplinary Applications*, eds. M. Gell-Mann and C. Tsallis (Oxford University Press, Oxford, 2002), to appear; in Annals of the Brazilian Academy of Sciences (2002), to appear [<http://www.scielo.br/scielo.php>] [cond-mat/0205571].
16. C. Beck, G.S. Lewis and H.L. Swinney, Phys. Rev. E **63**, 035303(R) (2001). See also C. Beck, Physica A **295**, 195 (2001) and *Phys. Rev. Lett.* **87**, 180601 (2001).
17. T. Arimitsu and N. Arimitsu, Physica A **305**, 218 (2002).
18. I. Bediaga, E.M.F. Curado and J. Miranda, Physica A **286**, 156 (2000).
19. A. Upadhyaya, J.-P. Rieu, J.A. Glazier and Y. Sawada, Physica A **293**, 549 (2001).
20. D.B. Walton and J. Rafelski, Phys. Rev. Lett. **84**, 31 (2000).
21. D.H. Zanette and P.A. Alemany, Phys. Rev. Lett. **75**, 366 (1995); C. Tsallis, S.V.F. Levy, A.M.C. de Souza and R. Maynard, Phys. Rev. Lett. **75**, 3589 (1995) [Erratum: **77**, 5442 (1996)]; D. Prato and C. Tsallis, Phys. Rev. E **60**, 2398 (1999); C. Tsallis and D.J. Bukman, Phys. Rev. E **54**, R2197 (1996); E.K. Lenzi, C. Anteneodo and L. Borland, Phys. Rev. E **63**, 051109 (2001).
22. M.A. Montemurro, Physica A **300**, 567 (2001).
23. L. Borland, Phys. Rev. Lett. (2002), in press.
24. C. Anteneodo, C. Tsallis and A.S. Martinez, Europhys. Lett. (2002), in press [cond-mat/0109203].
25. C. Tsallis, J.C. Anjos and E.P. Borges, [astro-ph/0203258].

26. P. Quarati, A. Carbone, G. Gervino, G. Kaniadakis, A. Lavagno and E. Miraldi, Nucl. Phys. A **621**, 345c (1997).
27. D.B. Ion and M.L.D. Ion, Phys. Rev. Lett. **81**, 5714 (1998); Phys. Rev. Lett. **83**, 463 (1999); Phys. Rev. E **60**, 5261 (1999); Phys. Lett. B **474**, 395 (2000); Phys. Lett. B **482**, 57 (2000); Phys. Lett. B **503**, 263 (2001).
28. F.A. Tamarit, S.A. Cannas and C. Tsallis, Eur. Phys. J. B **1**, 545 (1998).
29. C. Tsallis, J. Stat. Phys. **52**, 479 (1988); E.M.F. Curado and C. Tsallis, J. Phys. A **24**, L69 (1991) [Corrigenda: **24**, 3187 (1991) and **25**, 1019 (1992)]; C. Tsallis, R.S. Mendes and A.R. Plastino, Physica A **261**, 534 (1998).
30. S. Abe, [cond-mat/0206078].
31. A.K. Rajagopal and S. Abe, Phys. Rev. Lett. **83**, 1711 (1989).
32. P.T. Landsberg and V. Vedral, Phys. Lett. A **247**, 211 (1998); P.T. Landsberg, in *Nonextensive Statistical Mechanics and Thermodynamics*, eds. S.R.A. Salinas and C. Tsallis, Braz. J. Phys. **29**, 46 (1999).
33. C. Beck and F. Schlogl, *Thermodynamics of chaotic systems* (Cambridge University Press, Cambridge, 1993).
34. P. Bak, *How Nature Works : The Science of Self-Organized Criticality*, (Springer-Verlag, New York 1996); A. Bhowal, Physica A **247**, 327 (1997).
35. M. Baranger, *Chaos, Complexity, and Entropy: a Physics Talk for Non-Physicists*. <http://www.necsi.org/projects/baranger/cce.html>
36. C. Tsallis, A.R. Plastino and W.-M Zheng, Chaos, Solitons and Fractals **8**, 885 (1997). U.M.S. Costa, M.L. Lyra, A.R. Plastino and C. Tsallis, Phys. Rev. E **56**, 245 (1997), and M.L. Lyra and C. Tsallis, Phys. Rev. Lett. **80**, 53 (1998).
37. F. Baldovin and A. Robledo, [cond-mat/0205371].
38. F. Baldovin and A. Robledo, [cond-mat/0205356].
39. V. Latora and M. Baranger, Phys. Rev. Lett. **82**, 520 (1999).
40. A. N. Kolmogorov, Dokl. Akad. Nauk SSSR **119**, 861 (1958); **124**, 754 (1959).
41. Ya. B. Pesin, Russian Math. Surveys **32:4**, 55 (1977).
42. E. Ott, *Chaos in dynamical systems* (Cambridge University Press, 1993).
43. G.M. Zaslavsky and B.A. Niyazov, Phys. Rep. **283**, 73 (1997).
44. F. Baldovin and C. Tsallis, in progress.
45. C. Tsallis, G. Bentski, and R.S. Mendes, Phys. Lett. A **257**, 93 (1999).
46. F. Baldovin, C. Tsallis and B. Schulze, [cond-mat/0203595].
47. A. Bonasera, V. Latora and A. Rapisarda, Phys. Rev. Lett. **75**, 3434 (1995).
48. L. Casetti, M. Pettini and E.G.D. Cohen, Phys. Rep. **337**, 237 (2000).
49. L. Milanovic, H.A. Posch and W. Thirring, Phys. Rev. E **57**, 2763 (1998).
50. H. Koyama and T. Konishi, Phys. Lett. A **279**, 226 (2001); Y. Sota, O. Iguchi, M. Morikawa, T. Tatekawa and K. Maeda, Phys. Rev. E **64**, 056133 (2001).
51. M. Antoni and A. Torcini, Phys. Rev. E **57**, R6233 (1998); A. Torcini and M. Antoni, Phys. Rev. E **59**, 2746 (1999).
52. D. Lynden-Bell, Physica A **263**, 293 (1999).
53. D.H.E. Gross, *Microcanonical thermodynamics: Phase transitions in Small systems*, 66 Lectures Notes in Physics, World scientific, Singapore (2001).
54. M. D'Agostino et al., Phys. Lett. B **473**, 219 (2000).
55. P. Chomaz, in this volume.
56. M. Schmidt, R. Kusche, T. Hippler, J. Donges and W. Kronmueller, Phys. Rev. Lett. **86**, 1191 (2001).
57. J. Klafter and G. Zumofen, Phys. Rev. E **49**, 4873 (1994).
58. G. Parisi, Physica A **280**, 115 (2000).
59. P.G. Benedetti and F.H. Stillinger, Nature **410**, 259 (2001).

60. A. Coniglio, Physica A **306**, 76 (2002).
61. V. Latora, A. Rapisarda and C. Tsallis, Phys. Rev. E **64**, 056134 (2001).
62. V. Latora, A. Rapisarda and C. Tsallis, Physica A **305**, 129 (2002).
63. N.S.Krylov *Works on the Foundations of Statistical Physics*, translated by A.B. Migdal, Ya. G. Sinai and Yu. L. Zeeman, Princeton University Press (1979) and Nature **153**, 709 (1944).
64. A. Kudrolli and J. Henry, Phys. Rev. E **62**, R1489 (2000); Y-H. Taguchi and H. Takayasu, Europhys. Lett. **30**, 499 (1995).
65. M.F. Shlesinger, G.M. Zaslavsky and J. Klafter, Nature **363**, 31 (1993).
66. A. Rapisarda, C. Tsallis and A. Giansanti in preparation.
67. S. Abe, and N. Suzuki, [cond-mat/0204336].
68. M.A. Montemurro, F. Tamarit and C. Anteneodo [cond-mat/0205355].
69. E.P. Borges, and C. Tsallis, Physica A **305**, 148 (2002).

